Asymmetric and Speed-Dependent Capillary Force Hysteresis and Relaxation of a Suddenly Stopped Moving Contact Line

Dongshi Guan,[1] Yong Jian Wang,[1] Elisabeth Charlaix,[2] and Penger Tong[1]
[1]Department of Physics, Hong Kong University of Science and Technology, Clear Water Bay, Kowloon, Hong Kong
[2]Laboratoire Interdisciplinaire de Physique, Université Joseph Fourier, 140 rue de la physique, F-38402 Grenoble, France
(Received 29 June 2015; published 10 February 2016)

We report on direct atomic-force-microscope measurements of capillary force hysteresis (CFH) and relaxation of a circular moving contact line (CL) formed on a long micron-sized hydrophobic fiber intersecting a water-air interface. The measured CFH and CL relaxation show a strong asymmetric speed dependence in the advancing and receding directions. A unified model based on force-assisted barrier crossing is utilized to find the underlying energy barrier E_b and size λ associated with the defects on the fiber surface. The experiment demonstrates that the pinning (relaxation) and depinning dynamics of the CL can be described by a common microscopic framework, and the advancing and receding CLs are influenced by two different sets of relatively wetting and nonwetting defects on the fiber surface.

DOI: 10.1103/PhysRevLett.116.066102

Our understanding of fluid physics is often challenged at both the high velocity limit, where the nonlinear effect becomes dominant, and at the low velocity limit, where part of the fluid is pinned on the solid boundary. Contact angle hysteresis, where the motion of a contact line (CL) between a liquid interface and a solid substrate is pinned by the physical roughness and/or chemical inhomogeneity on the solid surface, is an example of the latter case [1–4]. The contact line pinning causes the contact angle θ between the liquid and solid surfaces to display some hysteresis; the CL cannot advance if θ is smaller than the advancing contact angle θ_a and cannot recede if θ is larger than the receding contact angle θ_r. For some low-energy surfaces, it was also found that the measured θ_a (and θ_r) depend on the speed u of the moving contact line (MCL) [5,6]. While considerable progress has been made recently in controlling the wettability of various textured solid surfaces [7,8], one still has a poor understanding of contact angle hysteresis on many ambient solid surfaces of interest [3].

A typical approach to modeling the speed dependence of $\theta_a(u)$ [or $\theta_r(u)$] is the molecular kinetic theory (MKT) [9], in which the motion of the CL is described as a thermally activated hopping event over an energy barrier E_b under the influence of the unbalanced capillary force [10], $f_{\rm un} = \gamma(\cos\theta_0 - \cos\theta_a)\lambda$, where θ_0 is the equilibrium contact angle, γ is the liquid-air interfacial tension, and λ is a typical size of defects on the solid surface. This capillary force increases the forward hopping rate k^+, reducing the backward hopping k^-, and gives rise to a net CL velocity, $u = (k^+ - k^-)\lambda$. Like many interfacial phenomena, the measurement of CL dynamics often involves contributions from the bulk fluid. A critical assumption made to link the MKT prediction to the bulk flow measurements is that the viscous dissipation of the bulk fluid is negligibly small at low speed. It was recently shown [11,12] that the dissipation of the MCL has the same velocity and viscosity dependence as that for the bulk flow but with a smaller numerical prefactor. As a result, many dynamic measurements of the CL contain significant contributions from the bulk flow, making the comparison between the MKT and experimental results inaccurate [12,13].

In this Letter, we report on a systematic study of the speed-dependent capillary force hysteresis (CFH) and relaxation of a suddenly stopped MCL over a hydrophobic surface grafted with a monolayer of Trichloro(1H,1H,2H,2H-perfluorooctyl)silane (FTS). In analogy to single-molecule pulling experiments [14], we use atomic-force microscopy (AFM) to directly measure the "rupture force" ΔF needed to break the "pinning bond" of a circular CL formed on a thin fiber surface for different load rates $\dot{f}$. The measured $\Delta F(\dot{f})$ is well described by a unified model for force-assisted barrier crossing [15,16], which establishes what happens microscopically at the CL to a macroscopically measurable quantity ΔF. Because forced barrier crossing does not involve any bulk flow, the comparison between the theory and an experiment is intrinsically more accurate.

Figures 1(a) and 1(b) show the working principle and the actual setup of a newly developed AFM-based capillary force apparatus. The "long needle" AFM involves a vertical glass fiber of diameter d in the range 0.4–4 μm and length 100–300 μm, which is glued onto the front end of a rectangular AFM cantilever (see the Supplemental Material [17] for more details). As a sensitive force apparatus, the long needle AFM measures the capillary force f acting on the circular CL formed between the liquid interface and the fiber surface. For a CL of length πd and contact angle θ_i, one has [18,19]

$$f = -\pi d\gamma\cos\theta_i, \tag{1}$$

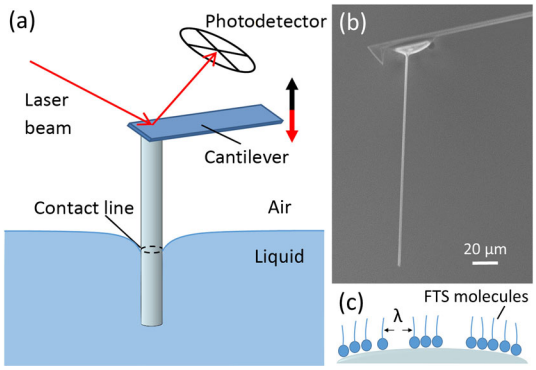

FIG. 1. (a) Sketch of the AFM-based capillary force apparatus. (b) A scanning electron microscope image of the actual hanging glass fiber of diameter $d \simeq 2.2$ μm and length 165 μm. (c) Sketch of the FTS coating on a glass fiber surface with defects of size λ (side view).

where the sign of f is defined as $f \leq 0$ for $\theta_i \leq 90°$ and $f > 0$ for $\theta_i > 90°$. Equation (1) is accurate when there is no hysteresis and θ_i takes the equilibrium value θ_0. With CFH, the values of θ_a (and θ_r) obtained from Eq. (1) may not be necessarily the same as those obtained using the conventional photographic method, as the latter may depend sensitively on the distance away from the CL at which the measurement is made [4]. Direct measurement of CFH at the CL does not have this experimental uncertainty. By moving the fiber up or down through the liquid interface at a constant speed u, one can accurately measure f as a function of time t or traveling distance $s = ut$. The fiber speed u is accurately controlled by the z-axis piezoelectric actuator of AFM in the range 0.5–100 μm/s with a travel distance s up to 25 μm. This wide variation range of u is essential for the study of the speed dependence of CFH. The corresponding capillary number $Ca \simeq \eta u/\gamma$ for water of viscosity $\eta = 1$ cP and $\gamma = 72.8$ mN/m is in the range

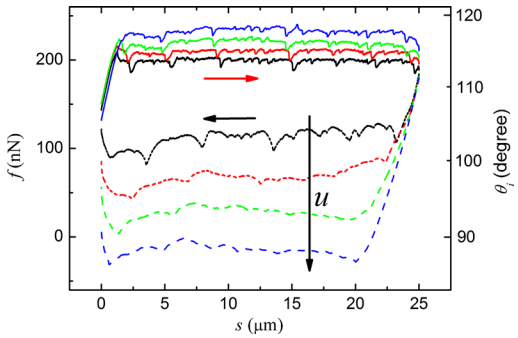

FIG. 2. Variations of the measured f and the corresponding contact angle θ_i [see Eq. (1)] when the glass fiber is pushed downward (advancing →, solid line) and is pulled upward (receding ←, dashed line) through a water-air interface. The measurements are made at fiber speed $u = 1$ (black lines), 3.5 (red lines), 10 (green lines), and 35 μm/s (blue lines), respectively. For clearance, each hysteresis loop is coded with a different color. The black long arrow indicates the direction of increasing u.

10^{-8}–10^{-6}, suggesting that the viscous effect is negligibly small.

Figure 2 shows typical CFH loops measured at different values of u when the glass fiber is pushed downward (advancing →) and is pulled upward (receding ←) through a water-air interface. Each CFH loop (color coded) consists of a sharp increase of f on the left and right sides of the loop followed by a horizontal fluctuating force on the top and bottom of the loop. Before the start of the motion, the fiber was already partially immersed in the water and the contact line was pinned on the fiber surface. When the fiber advances (→), the pinned interface is stretched, causing a linear increase in f with the distance traveled s, as shown by a straight line at the beginning of the loop. When the restoring force becomes larger than a critical value, f_a, the CL depins and begins a steady stick-and-slip motion, as evidenced by the horizontal fluctuations in the force curve. It is seen that the value of f_a increases with the fiber speed u. When the direction of motion is reversed (←), a similar pinning-depinning process is repeated and the obtained values of f_r show a stronger u dependence.

Another interesting phenomenon observed in the system is that when the moving fiber at its steady state with speed u suddenly stops at time $t = 0$, the measured $f(t)$ starts to relax with t and reaches an asymptotic value f_0. Figure 3 shows how the measured $f(t)$ changes with t for a moving fiber in the advancing (red line) and receding (black line) directions with an initial speed $u = 20$ μm/s at $t = 0$. The relaxation of $f(t)$ is asymmetric with a large amplitude relaxation in the receding direction. Furthermore, the relaxation of $f(t)$ has two different asymptotic values, $(f_0)_a$ and $(f_0)_r$, respectively, in the advancing and receding directions. The inset of Fig. 3 shows how the relaxation of

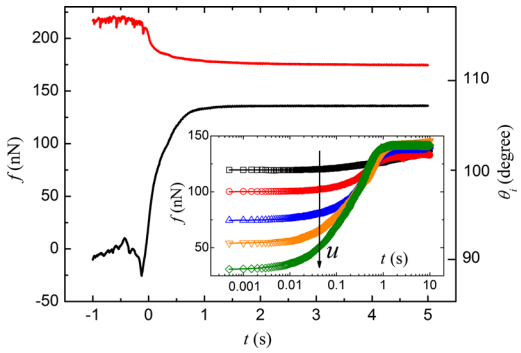

FIG. 3. Relaxation of the measured capillary force $f(t)$ as a function of time t for a moving fiber through a water-air interface in the advancing (red line) and receding (black line) directions with an initial speed $u = 20$ μm/s at $t = 0$. The corresponding value of $\theta_i(t)$ [see Eq. (1)] is marked on the right vertical axis. The inset shows the relaxation of $f(t)$ in the receding direction with different initial speeds at $t = 0$: $u = 1$ (black), 2 (red), 5 (blue), 10 (orange), and 20 μm/s (green). The black long arrow points in the direction of increasing u. The solid lines show the fits to Eq. (5).

$f(t)$ in the receding direction changes with different initial speeds u at $t = 0$. It is found that the decay rate of $f(t)$ depends sensitively on u, whereas the value of $(f_0)_r$ does not change much with u. Similar results are also found in the advancing direction (see the Supplemental Material [20] for more details). A similar $\ln t$ relaxation was also observed in dynamic wetting of colloidal particles at a liquid interface [13]. Evidently, the relaxation of $f(t)$ is a reversal process of CL depinning.

Figure 4 shows the u dependence of the measured rupture force ΔF needed to break the CL pinning (per unit length). Here, ΔF is defined as

$$\Delta F_i \equiv |f_i - (f_0)_i|/(\pi d), \tag{2}$$

where f_i is the mean value of the measured capillary force at its steady state in the advancing ($i = a$) or receding ($i = r$) direction, as shown in Fig. 2, and $(f_0)_i$ is the corresponding value after relaxation, as shown in Fig. 3. The measured ΔF_i shows an approximate $\ln u$ dependence, and its slope in the receding direction is much larger than that in the advancing direction.

To model the depinning process of the CL, we consider a CL which is pinned by $N = (a/\lambda)\pi d$ defects, where a/λ is the defect line density, with $a \leq 1$ being a numerical constant and λ a typical defect size, as shown in Fig. 1(c). The average fracture force needed to break the pinning bound between the CL and a single defect is thus $\delta f \simeq \Delta F(\lambda/a)$. The main effect of external pulling in the depinning process is to lower the energy barrier of the trapping (or blocking) potential $U(z)$ associated with the defect. Under a constant force f, the effective potential becomes $U(z) - fz$ and the escape rate over the energy barrier (depinning) is given by [15,16]

$$K(f) = K_0(1 - f/f_c)^{b-1} e^{-E_b(1-f/f_c)^b/k_BT}, \tag{3}$$

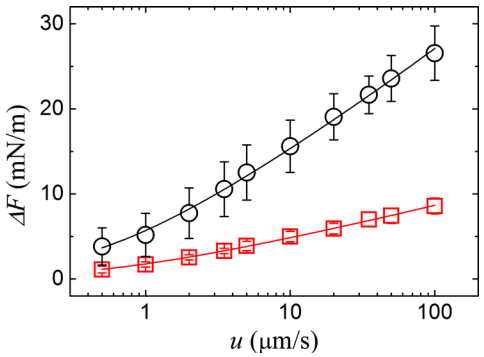

FIG. 4. Measured rupture force ΔF as a function of fiber speed u in the advancing (red squares) and receding (black circles) directions. The error bars show the standard deviation of the measurements. The solid lines are the fits to Eq. (4) with $(E_b)_a = 14.6k_BT$ and $\lambda_a = 1.30$ nm in the advancing direction and $(E_b)_r = 16.8k_BT$ and $\lambda_r = 0.73$ nm in the receding direction.

where K_0 is the attempt frequency, E_b is the intrinsic energy barrier of $U(z)$, and $f_c = 2bE_b/\lambda$ is the critical force at which the barrier to escape vanishes. The parameter b selects a particular form of the potential $U(z)$. Here, we choose $b = 3/2$ for a generic liner-cubic potential [21,22].

When the CL is pinned on a fiber surface moving at constant speed u, the liquid interface is continuously stretched, which exerts a time-dependent pulling force, $f = k_s ut = \dot{f}t$, on the CL, with k_s being the spring constant of the liquid interface. As time t increases, the effective energy barrier is continuously reduced by a factor of $(1 - \dot{f}t/f_c)^b$ and the escape rate $K(f)$ increases. If the normalized loading rate $\dot{f}/f_c$ is much larger than the thermal activation rate $K(f = 0)$ in Eq. (3), the force-assisted barrier crossing is determined primarily by the mechanical pulling, without much help from thermal fluctuations. In this case, the fracture force needed is $\delta f = f_c$. If $\dot{f}/f_c$ is smaller than $K(0)$, thermal fluctuations can help the barrier crossing and the fracture force needed is less than f_c. In this case, one has [16,23]

$$\Delta F \simeq \frac{a}{\lambda} f_c \left\{ 1 - \left[1 - \frac{k_BT}{E_b} \ln\left(1 + \frac{e^{-\alpha}\dot{f}/f_T}{2K_0 e^{-E_b/k_BT}} \right) \right]^{2/3} \right\}, \tag{4}$$

where $f_T = k_BT/\lambda$ is the thermal force and $\alpha \simeq 0.577$ is the Euler constant. Equation (4) establishes a direct link between the macroscopically measurable quantity ΔF and the microscopic details of the defect, such as E_b and λ. By varying $\dot{f}$ (or the speed u), one obtains the dynamic force spectroscopy [14] of CL depinning.

For defects on a high-energy surface, such as a glass surface, their energy barrier tends to be high [33], so that their thermal activation rate $K(0)$ is low compared to a typical loading rate $\dot{f}/f_c$. On the other hand, for defects on a low-energy surface, such as a FTS-coated fiber surface, their energy barrier is small as the overall energy scale is reduced and thus their $K(0) \gtrsim \dot{f}/f_c$. This explains why we observe the u dependence of CFH on a FTS-coated surface but not on a glass surface [34]. The solid lines in Fig. 4 show the fits to Eq. (4), with E_b and λ being used as two fitting parameters. The value of other parameters in Eq. (4), including a, k_s, and K_0, has been predetermined in the experiment (see the Supplemental Material [23] for more details). It is seen that Eq. (4) fits the data well with the fitting results given in the caption.

To keep the CL moving at a constant speed u, an extra force is needed in order to overcome the extra dissipation introduced by the defects. This extra force is the unbalanced capillary force, $f_{\rm un} = \pi d\gamma|\cos\theta_0 - \cos\theta_i|$, which is generated when the liquid interface near the CL changes its contact angle from θ_0 to θ_i. Once the motion of the CL is stopped, the unbalanced capillary force $f(t)$ will relax from its initial value $f(0) = f_a$ (or f_r) at $t = 0$ to its final

value f_0 at a large t. Physically, this relaxation process is accomplished by the CL moving along the fiber over a small distance $z(t)$ with speed $u(t) = \dot{z}(t)$ back to its pinning state (minimum-energy state). As shown in Fig. 3, the local pinning state in the advancing direction differs from that in the receding direction, giving rise to two different asymptotic values of $(f_0)_a$ and $(f_0)_r$. Because the relaxation is accomplished by thermal fluctuations, the value of f_0 is determined primarily by those defects with large energy barriers, which prevent the CL from further relaxing to a common equilibrium value $f_0 = \pi d\gamma \cos\theta_0$. With this understanding, we find the relaxation of $f(t) = k_s z(t)$ can also be described by Eq. (4).

In the limit of $E_b/k_BT \gg 1$, Eq. (4) can be simplified into the Bell form [16,35], $\Delta F(t) \simeq (2a/\lambda) f_T \ln[1 + \beta\dot{z}(t)]$, where $\beta = e^{-\alpha} k_s/[2 f_T K_0 \exp(-E_b/k_BT)]$ and $\Delta F(t) = \mp[k_s z(t) - f_0]/\pi d$. Here, the minus sign is used for advancing and the plus sign for receding. By integrating this first-order differential equation on both sides, we find the final solution of $z(t)$ in the limit $\beta\dot{z} \gg 1$ (see the Supplemental Material [23] for more details),

$$f(t) = \mp \frac{2a\pi d}{\lambda} f_T \ln(\Gamma t + c) + f_0, \tag{5}$$

where the relaxation rate $\Gamma = K_0 \exp(-E_b/k_BT)/[e^{-\alpha}\pi d(a/\lambda)]$ and the integration constant $c(u) = \exp\{\mp[f(0) - f_0]/(2a\pi d f_T/\lambda)\}$, which depends on the initial speed u. Equation (5) uses the same set of parameters as those in Eq. (4) to describe the relaxation of $f(t)$.

The solid lines in the inset of Fig. 3 show the fits to Eq. (5) using E_b and λ as two fitting parameters. The value of other parameters in Eq. (5) is kept the same as that used in Eq. (4). It is seen that Eq. (5) fits the data well over almost four decades of decay time t with the fitting results: $(E_b)_a = 15.4 \pm 0.9 k_BT$ and $\lambda_a = 1.41 \pm 0.28$ nm in the advancing direction and $(E_b)_r = 16.8 \pm 0.8 k_BT$ and $\lambda_r = 0.76 \pm 0.14$ nm in the receding direction. The error bars quoted here are the standard deviations obtained from the measurements with ten different speeds (see the Supplemental Material [23] for more details). The fitting results obtained from Fig. 3 are in good agreement with those from Fig. 4. Using the fitted values of E_b and λ, we find the normalized fracture force $\delta f/f_c$ (per defect) varies in the range of 0.05–0.3 with the fiber speeds used in the experiment. This result is close to our expectation, $\delta f/f_c \simeq 1/3$, based on the estimated defect energy [6] $E_b \simeq \gamma\lambda^2 |\cos\theta_i - \cos(\theta_0)_i|$. The above results demonstrate that the speed dependence of CFH and relaxation of a MCL are controlled by the same microscopic mechanism, and our model captures the essential physics.

An important feature shown in Figs. 2–4 is that the pinning (relaxation) and depinning dynamics of the advancing CL is very different from that of the receding CL. They have different speed dependence and different asymptotic values of f_0, suggesting that the advancing and receding CLs have different pinning (metastable) states. It was found in a recent experiment [34] that a solid surface often contains two sets of coexisting and spatially intertwined defects with opposite natures. The two types of defects may be generated either by the positive and negative fluctuations of chemical heterogeneity relative to the mean or by the physical roughness of the surface with grooves and ridges. The CL is pinned primarily by the nonwetting (repulsive) defects in the advancing direction and by the wetting (attractive) defects in the receding direction. These two different types of defect landscapes therefore produce two different capillary forces, f_a and f_r (or θ_a and θ_r), depending on the moving direction of the CL. This "composite model" is further supported by our finding that two sets of parameters E_b, λ, and f_0 are needed to describe the pinning and depinning dynamics of the advancing and receding CLs, respectively.

For a FTS-coated glass surface, one usually can only achieve 70%–90% of its maximum packing density [36], leaving uncovered holes on the otherwise hydrophobic surface, as sketched in Fig. 1(c). These uncovered holes thus become wetting defects to the CL for the water-air interface. Because the FTS-coated fiber surface has more wetting defects, the CL is pinned predominantly in the receding direction. This explains qualitatively why the observed u dependence of CFH and CL relaxation is asymmetric with the effect on the receding CL being much larger than that on the advancing CL. Furthermore, we find that the critical force $(f_c)_r \simeq 3(E_b)_r/(\lambda_a)_r$ in the receding direction is more than twice as large as $(f_c)_a$ in the advancing direction.

We thank H.-Y. Chen, T.-Z. Qian, and X.-G. Ma for the illuminating discussions. This work was supported in part by RGC of Hong Kong SAR under Grant No. C6004-14G (P. T.) and by ANR Blue Energy, Grant No. ANR-14-CE05-0017-02 (E. C.).

[1] P.-G. de Gennes, Rev. Mod. Phys. **57**, 827 (1985).
[2] L. Leger and J.-F. Joanny, Rep. Prog. Phys. **55**, 431 (1992).
[3] E. L. Decker and S. Garoff, J. Adhes. **63**, 159 (1997).
[4] D. Bonn, J. Eggers, J. Indekeu, J. Meunier, and E. Rolley, Rev. Mod. Phys. **81**, 739 (2009).
[5] A. Prevost, E. Rolley, and C. Guthmann, Phys. Rev. Lett. **83**, 348 (1999).
[6] E. Rolley and C. Guthmann, Phys. Rev. Lett. **98**, 166105 (2007).
[7] D. Quéré, Annu. Rev. Mater. Res. **38**, 71 (2008).
[8] M. Ramiasa, J. Ralston, R. Fetzer, and R. Sedev, Adv. Colloid Interface Sci. **206**, 275 (2014).
[9] T. D. Blake and J. M. Haynes, J. Colloid Interface Sci. **30**, 421 (1969).
[10] J. Snoeijer and B. Andreotti, Annu. Rev. Fluid Mech. **45**, 269 (2013).
[11] S. Guo, M. Gao, X. Xiong, Y. J. Wang, X. Wang, P. Sheng, and P. Tong, Phys. Rev. Lett. **111**, 026101 (2013).

[12] S. Guo, C. H. Lee, P. Sheng, and P. Tong, Phys. Rev. E **91**, 012404 (2015).
[13] D. M. Kaz, R. McGorty, M. Mani, M. P. Brenner, and V. N. Manoharan, Nat. Mater. **11**, 138 (2012).
[14] E. Evans, Annu. Rev. Biophys. Biomol. Struct. **30**, 105 (2001).
[15] H. J. Lin, H. Y. Chen, Y. J. Sheng, and H. K. Tsao, Phys. Rev. Lett. **98**, 088304 (2007).
[16] R. W. Friddle, Phys. Rev. Lett. **100**, 138302 (2008).
[17] See Supplemental Material, Sec. I at http://link.aps.org/supplemental/10.1103/PhysRevLett.116.066102 for experimental details.
[18] J.-M. Di Meglio and D. Quéré, Europhys. Lett. **11**, 163 (1990).
[19] M. M. Yazdanpanah, M. Hosseini, S. Pabba, S. M. Berry, V. V. Dobrokhotov, A. Safir, R. S. Keynton, and R. W. Cohn, Langmuir **24**, 13753 (2008).
[20] See Supplemental Material, Sec. II at http://link.aps.org/supplemental/10.1103/PhysRevLett.116.066102 for more experimental results and data analysis.
[21] A. Garg, Phys. Rev. B **51**, 15592 (1995).
[22] X.-G. Ma, P.-Y. Lai, B. J. Ackerson, and P. Tong, Soft Matter **11**, 1182 (2015).
[23] See Supplemental Material, Sec. III at http://link.aps.org/supplemental/10.1103/PhysRevLett.116.066102, which includes Refs. [24–32], for more discussions on the theoretical model.
[24] J.-M. Meglio and D. Quéré, Europhys. Lett. **11**, 163 (1990).
[25] M. Delmas, M. Monthioux, and T. Ondarcuhu, Phys. Rev. Lett. **106**, 136102 (2011).
[26] P. Silberzan, L. Leger, D. Ausserre, and J. J. Benattar, Langmuir **7**, 1647 (1991).
[27] J. B. Brzoska, I. B. Azouz, and F. Rondelez, Langmuir **10**, 4367 (1994).
[28] X.-M. Xiong, S. Guo, Z.-L. Xu, P. Sheng, and P. Tong, Phys. Rev. E **80**, 061604 (2009).
[29] S. Guo, X.-M. Xiong, Z.-L. Xu, P. Sheng, and P. Tong, Chin. Phys. B **23**, 116802 (2014).
[30] J. L. Hutter and J. Bechhoefer, Rev. Sci. Instrum. **64**, 1868 (1993).
[31] L.-H. Tang, in *Encyclopedia of Complexity and Systems Science*, edited by R. A. Meyers (Springer, New York, 2009).
[32] P. Le Doussal and K. J. Wiese, Phys. Rev. E **82**, 011108 (2010).
[33] P.-G. de Gennes, F. Brochard-Wyart, and D. Quere, *Capillarity and Wetting Phenomena* (Springer, New York, 2004).
[34] Y. J. Wang, S. Guo, H.-Y. Chen, and P. Tong (to be published).
[35] G. I. Bell, Science **200**, 618 (1978).
[36] T. M. Mayer, M. P. de Boer, N. D. Shinn, P. J. Clews, and T. A. Michalske, J. Vac. Sci. Technol. B **18**, 2433 (2000).